Journal of Energy Storage 73 (2023) 109210

Contents lists available at ScienceDirect

Journal of Energy Storage

journal homepage: www.elsevier.com/locate/est

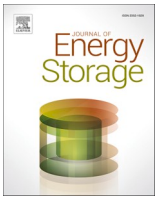

Research papers

SiO_x coated graphite with inorganic aqueous binders as high-performance anode for lithium-ion batteries

Shivam Trivedi [a,*], Sirshendu Dinda [a], Yushu Tang [b,c], Stefan Fuchs [a], Venkat Pamidi [a], Helge S. Stein [a,b], Anji Reddy Munnangi [d], Maximilian Fichtner [a,e,**]

[a] Helmholtz Institute Ulm (HIU), 89081 Ulm, Germany
[b] Institute of Physical Chemistry (IPC), Karlsruhe Institute of Technology (KIT), 76021 Karlsruhe, Germany
[c] Karlsruhe Nano Micro Facility (KNMF), Karlsruhe Institute of Technology (KIT), 76021 Karlsruhe, Germany
[d] Faculty of Science and Engineering, Swansea University, Swansea SA1 8EN, United Kingdom
[e] Institute of Nanotechnology, Karlsruhe Institute of Technology, 76021 Karlsruhe, Germany

ARTICLE INFO

Keywords:
Lithium-ion batteries
Aqueous binders
Inorganic binders
Graphite coatings

ABSTRACT

Inorganic aqueous binders (IAB) are an emerging class of aqueous binders. They offer exceptional physico-chemical properties like intrinsic ionic conductivity, high thermal stability (>1000 °C), and environmental benignity making them attractive. In a previous study, we found that graphite anode shows improved electrochemical performance with these binders as compared to conventional PVDF binder for lithium-ion batteries (LIB). However, the cyclic performance of graphite-IAB at a higher rate (e.g., 1C) showed a declining trend. We attributed it to the poor binding strength between graphite and IAB due to insufficient functional groups in graphite. Therefore, in this report SiO_x-based surface coatings of graphite are employed to improve its rate capability with silicate-based IAB by providing functional silicon oxide polymorphs on the coated graphite as an intermediate layer. The nature and structural arrangement of these coatings are investigated by tip-enhanced Raman spectroscopy (TERS), X-ray photoelectron spectroscopy (XPS), and transmission electron microscopy (TEM). Optimized SiO_x-coated graphite (GS) with sodium metasilicate binder leads to excellent cyclic stability with a capacity retention of >90 % at 20C for >4000 cycles. A high specific capacity of >315 $mAhg^{-1}$ at 2C, stable for over 1000 cycles, is achieved for GS with IAB. The improved performance of the coated graphite is attributed to ameliorated binding with IAB as well as stable solid electrolyte interphase. We propose inorganic aqueous binders in combination with SiO_x-coated graphite as an approach to realize a stable anode for LIB.

1. Introduction

Graphite is a well-known commercial anode for lithium-ion batteries (LIB). It has a characteristic sp^2 hybridized layered carbon structure held together by weak van-der Waals forces. It has a flake like particle morphology with two kinds of surfaces – edge planes and basal planes [1]. Vast research efforts have been dedicated to study graphite in LIB due to its advantages like low cost, abundance, high energy density and cycle life [2,3]. However, only limited efforts were made to explore the role of binders. For a long time, it was believed that they are inactive ingredients which only have an adhesive function [4,5].

Conventional binders such as polyvinylidene fluoride (PVDF) necessitate the use of toxic and expensive solvent like *N*-methyl pyrrolidone (NMP) [6]. Moreover, the weak van der Waals forces present between PVDF and the active material fail to bond adequately and maintain electrode integrity during long cycling, leading to capacity fading [7]. Besides, the transition towards sustainable and low cost energy devices has motivated to study water-soluble (aqueous) binders and assess their role and contribution in electrochemical performance [4,5,8]. In this regard, organic aqueous binders such as carboxy methyl cellulose (CMC) and its mixture (CMC-SBR) with styrene butadiene rubber (SBR), have been found to work well with graphite-based anodes [9–12]. The carboxyl (—COOH) and hydroxy (—OH) groups on these binders generate strong hydrogen bonds, leading to improved binding of electrode components and eventually lead to stable electrochemical performance [13]. Apart from these binders, IAB have also been known

* Corresponding author.
** Correspondence to: M. Fichtner, Institute of Nanotechnology, Karlsruhe Institute of Technology, 76021 Karlsruhe, Germany.
E-mail addresses: shivam.trivedi@kit.edu (S. Trivedi), m.fichtner@kit.edu (M. Fichtner).

https://doi.org/10.1016/j.est.2023.109210
Received 12 August 2023; Received in revised form 2 October 2023; Accepted 5 October 2023
Available online 7 October 2023

for over a decade. However, lack of detailed and systematic study did not reveal the full potential of these binders.

Recently, we investigated several inorganic aqueous binders (IAB) and studied them with different sodium and lithium-based electrode material, which reignited the interest [14]. Most of these binders performed well with hard carbon but failed to show stable cycling with graphite although both are carbon-based materials. Graphite displayed optimum capacities at 0.1C but at higher rate of 1C, poor rate capability was observed [14]. We concluded that these binders hydrolyse and develop —OH groups during aqueous processing. On electrode drying, the —OH and —COOH groups of active material such as hard carbon may undergo condensation reaction with —OH groups of IAB, thereby creating a bond between active material and binder [14,15]. The dearth of surface functional groups in graphite limits its binding with IAB. Therefore, surface coating or incorporation of surface functional groups on graphite would be necessary to improve electrochemical performance of graphite with IAB. In this regard, thin silicon oxide (SiO_x) coatings on graphite could be helpful by providing two-fold assistance: to bind with silicate based IAB through chemical interlinkage and preventing exfoliation/structural degradation during prolonged electrochemical cycling.

Coating of graphite is a known technique to improve electrochemical performance and is widely reported in the literature [16]. Graphite has reactive edges along with heteroatomic impurity (e.g. O, H etc.) in its basal planes and edge sites which may trigger electrolyte decomposition and irreversible capacity loss [17]. Thin layer coatings and surface modifications of graphite with materials such as carbon [18], metals [19,20] metal oxides [21] and ion conducting polymers [22] etc. have been reported to suppress irreversible intercalation of solvated species, side reactions and exfoliation of graphite during cycling. Moreover, these surface coatings can also act as an artificial solid electrolyte interphase (SEI) which can have better compatibility with electrolytes as compared to pristine graphite [16]. SiO_2 coatings have been utilized to improve thermal conductivity and electrical insulation properties of graphite (composites) for electronic devices [23] but comparatively few reports [24–26] are available for battery electrode materials, probably because they compromise with electronic conductivity. The SiO_2 coated graphite was reported by Yong et al. [26] to show ~16 % improvement in capacity retention (CR) after 40 cycles at 0.1 $mAcm^{-2}$. This increase in CR was attributed to improved SEI due to a steric network of SiO_2 on the coated graphite.

To combine the exceptional properties of IAB (aqueous processability, high binding strength and ionic conductivity) with that of graphite, a thin layer SiO_x surface coating on graphite could be beneficial. These coatings may act simultaneously as a surface protector and interlinkage provider to IAB via physicochemical interaction.

Hence, in this study, we report the role of SiO_x coatings on graphite and investigate their physicochemical properties and electrochemical performance with different binders. Firstly, SiO_x coatings on graphite were produced using wet chemical method. This SiO_x coated graphite (GS) along with pristine graphite (G) was studied with three IAB: lithium dihydrogen phosphate (LiH_2PO_4: LHPO), lithium polysilicate ($Li_2Si_5O_{11}$: LPS) and sodium metasilicate (Na_2SiO_3: SMS). For reference, the electrochemical performance with three well-known organic binders, PVDF, CMC and CMC-SBR (1:1 wt%), has also been evaluated. Overall, the electrochemical performance of graphite is compared against coated graphite using six different binders. In this report, we attempt to improve the rate capability of graphite using combination of surface coating and suitable binders.

2. Experimental

2.1. Materials

Commercial graphite (pristine graphite: G) was purchased from C-Nergy™. All the binders used in this report are commercially available. The details and specifications of all chemicals used are provided in the supporting information (SI), Table S1.

2.2. Thin layer coating on graphite

SiO_x coating on graphite was carried out by polyvinyl pyrrolidone (PVP: $(C_6H_9NO)_n$) assisted sol-gel reaction as reported in the literature [27]. In brief, 5 g of graphite and 0.5 g (10 wt%) of PVP were added to 70 mL ethanol and then stirred at 500 rpm for 3 h. This step leads to physical adsorption of PVP on graphite surface. After this, 10 μL of tetra ethyl orthosilicate (TEOS) and 830 μL of ammonia solution (NH_4OH) were added (1:3 wt%) to the above dispersion and continuous stirring was maintained for 12 h at same rate. The final product was washed with ethanol: water (1:1) mixture until neutral pH. The washing step removes excess NH_4OH and loosely bonded PVP from the graphite surface. The coated graphite (GS) thus obtained was heated at 60 °C for 12 h under vacuum. Similarly, coatings were also prepared by using two times (GS-2) and five times (GS-5) TEOS concentrations but keeping PVP concentration fixed at 10 wt% with respect to graphite.

2.3. Electrochemical testing

In the first step, uniform dispersions of binders were obtained in a suitable solvent by continuous stirring. Aqueous binders (CMC, CMC-SBR, LHPO, LPS and SMS) were dispersed in deionized water (Milli-Q® Water Purification System) whereas PVDF was dispersed in NMP. The desired quantity of the binder dispersion was added to the active material (G/GS) and mixed in a high-speed mixer (Thinky™ ARE-250) at 2000 rpm for 10 min. The obtained slurry was coated on copper current collector using doctor blade technique and dried at 80 °C for 12 h, followed by 120 °C for 4 h. Circular discs of 12 mm diameter were cut using an electrode cutter. Average mass loading was maintained between 1 and 1.5 $mg{\cdot}cm^{-2}$ for all electrodes.

Swagelok type cells were fabricated in a half cell configuration inside an argon filled glove box (<0.1 ppm H_2O, <0.1 ppm O_2). The graphite-binder electrode was taken as the working electrode and lithium metal pressed on steel current collector was used as the counter electrode. Two borosilicate glass (GF/C) separators soaked in liquid electrolyte (LE) was used as the separating layer between the two electrodes. For each cell, 60 μL of 1 M LiTFSI in EC: DMC (1:1) was used as the LE. The cells were first allowed to rest for 6 h to stabilize reach a steady state condition and then cycled at 25 °C using a Biologic BCS-805 battery cycler. The cells were discharged until 0.0 V followed by charging until 3.0 V at constant current (C-rate). In case of cycling at 1C or more, lower potential was increased to 1 mV. These discharge-charge cycles were repeated multiple times to estimate cyclic performance and rate capabilities at different C-rates. Electrochemical impedance spectroscopy (EIS) measurements were carried out between 100 mHz and 1 MHz range with an AC amplitude of 10 mV.

2.4. Methods

2.4.1. X-ray diffraction (XRD)

For XRD measurement, samples were placed between two polyimide films in air atmosphere and scanned in a 2θ range of 5–50° with a scan speed of 1° min^{-1}. XRD data was collected using *STOE* - STADI P diffractometer equipped with a molybdenum Kα radiation source (50 kV/40 mA, λ = 0.709 Å) in the transmission mode.

2.4.2. Thermogravimetric analysis (TGA)

TGA of the graphite & coated graphite samples along with PVP were carried out in argon atmosphere from 40 to 1000 °C at the rate of 10 °C/min in TA instruments Q5000.

2.4.3. Raman spectroscopy

Micro-Raman spectra were collected by inVia™ confocal Raman

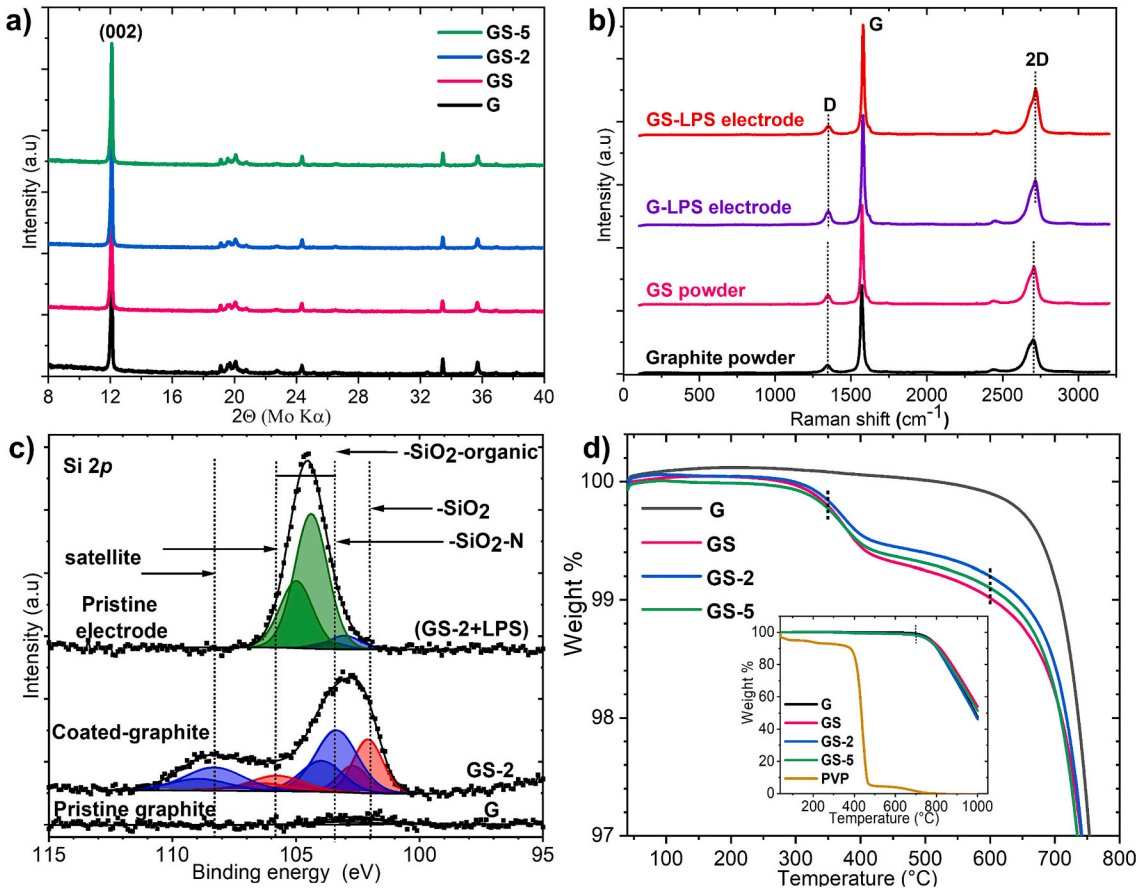

Fig. 1. Characterization of graphite, coated graphite & their pristine electrodes. a) XRD of graphite and coated graphite powders. b) Raman of (coated) graphite powder and electrode with LPS binder. c) XPS of graphite, coated graphite and their pristine electrode with LPS binder. d) TGA of graphite, coated graphite samples and PVP powder. G = pristine graphite, GS: coated graphite, GS-2: coated graphite prepared using 2 times TEOS concentration, GS-5: coated graphite prepared using 5 times TEOS concentration.

microscope (RENISHAW) set with 532 nm excitation laser. The average laser power was kept at ~1 mW and exposure times varied from 20 s to 120 s depending on sample response.

The tip-enhanced Raman spectroscopy (TERS) setup used here is a commercial optical setup, where a Bruker nano surface Innova-IRIS scanning probe microscope (SPM) system is optically coupled with Renishaw's inVia Raman microscope. The TERS system is installed in an inert glovebox. The scanning tunneling microscope (STM) is aligned in a side illumination geometry with the Raman microscope.

The TERS experiment was performed in STM mode and a TERS-STM gold tip from Bruker was used. To get the STM image of the surface of coated material (2 × 2 μm^2), a constant current mode of 2 nA was selected, keeping the tip bias at 0.5 V. A long focusing distance objective (50×, 0.42 NA) was used for tightly focusing on the TERS tip apex whereas the 633 nm excitation laser was used to illuminate the tip. The TERS measurements were performed using 1 mW average laser power, 1 s exposure time and three acquisitions for acquiring Raman spectrum.

2.4.4. X-ray photoelectron spectroscopy (XPS)

XPS measurements were performed with a SPECS EnviroESCA unit having a monochromatic Al K_α source (1486.71 eV) and high-resolution spectra were recorded at a pass energy of 30 eV. The NAP-XPS is part of the platform for accelerated electrochemical energy storage Research (PLACES/R) at Helmholtz Institute Ulm [28].

2.4.5. Electron microscopy

Microstructural investigation was performed by Thermoscientific Spreo 2, scanning electron microscope (SEM) using an accelerating voltage between 5 and 10 kV. Following, morphological and structural investigation of the graphite was conducted by high-resolution transmission electron microscope (HRTEM) with a ThermoFisher Themis 300 operating at a working voltage of 300 kV. It was equipped with high-angle annular dark-field scanning transmission electron microscopy (HAADF-STEM) coupled with energy dispersive X-ray spectroscopy (EDX) for the HAADF imaging and elemental distribution analysis.

3. Results and discussion

3.1. Physicochemical characterization

Fig. 1a shows the XRD patterns of G and GS prepared using different concentrations of TEOS. Graphite showed a characteristic peak at 2θ = 12.09° which corresponds to a d-spacing (002) of 0.338 nm. The coated graphite samples exhibited similar XRD peaks, suggesting no noticeable change in bulk structure of graphite during sol-gel preparation of thin layer coating.

Raman measurements were carried out for powders of graphite (G) and coated graphite (GS) along with their electrode (pristine) counterparts with LPS binder. Fig. 1b shows that their Raman spectra is overlapped precisely along the prominent bands of graphite, at 1350 cm^{-1}, 1580 cm^{-1}, and 2716 cm^{-1} corresponding to D, G and 2D bands respectively [29]. The I_D/I_G ratio remained unaltered at 0.9 even after the coating. This proved that graphite lattice remained virtually unmodified upon physical and chemical treatment of graphite during coating and electrode preparation process. The presented Raman spectra failed to capture any signal other than the graphitic structure, revealing

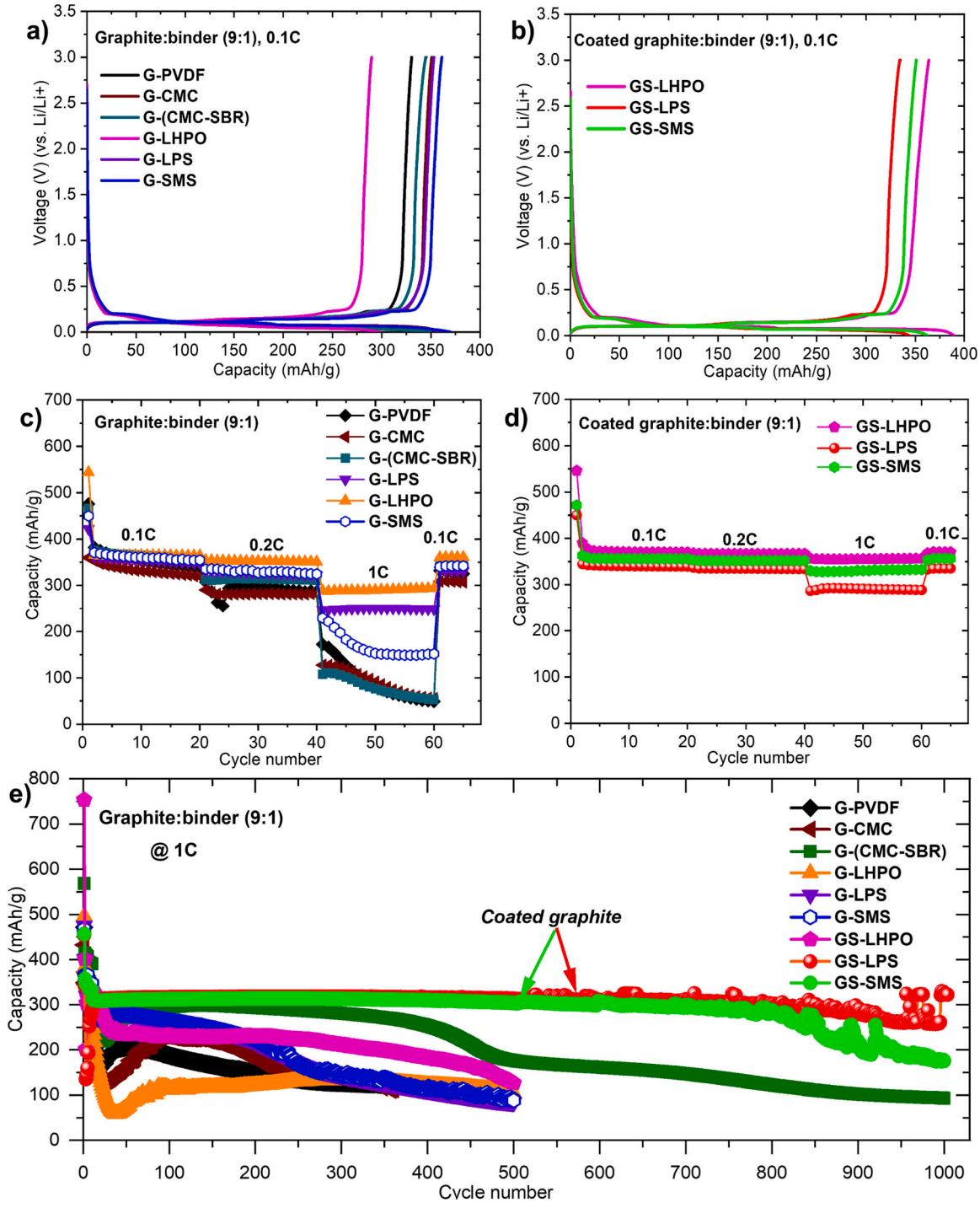

Fig. 2. Electrochemical performance of graphite (G) and coated graphite (GS) with 10 wt% of different binders. a) 2nd discharge-charge profile of graphite. b) 2nd discharge-charge profile of coated graphite. c) Rate capability of graphite. d) Rate capability of coated graphite. e) Cyclic performance of graphite and coated graphite at 1C. The corresponding Coulombic efficiency plots are given in Fig. S5. The electrochemical performance is summarized in Tables S2 & S3 in the SI and SEM of cycled electrodes in given in Fig. S6.

no information on chemical and structural changes. This could be due to the presence of very thin layer of SiO_x on graphite, the Raman effect might be weak and hence its signals were not detected. Therefore, tip-enhanced Raman spectroscopy (TERS) was used to examine these coatings, the details of the findings are presented in Section 3.3.

XPS was performed on graphite, coated graphite and their pristine electrodes with LPS binder. Fig. 1c shows XPS of graphite (G), coated graphite (GS-2) and their electrode with LPS binder. In the Si 2*p* region two sets of doublets were observed. The doublet at 102.1/102.7 eV was assigned to Si bound to PVP and the doublet at 103.4/104.0 eV was assigned to Si directly bound to graphite. The doublet at 102.1 eV and 102.7 eV was accompanied by a shakeup satellite peak at 108.3 eV indicating an interaction of the unfilled 3*d* orbitals of Si with the π-orbitals of the aromatic heterocycle present in PVP that extends the final-state orbital to the oxygen as indicated by an O 1*s* satellite peak at 537.7 eV [30]. The C 1*s*, O 1*s* and N 1*s* spectra are shown in the SI, Fig. S1. The C 1*s* feature corresponding to graphitic carbon was observed at 284.4 eV and remained unchanged for graphite, coated graphite and its electrode

with LPS binder [31]. This confirmed that the coating and aqueous processing did not change the graphite lattice. In the O 1*s* region two main peaks were observed at 531.9 eV and 533.5 eV assigned to terminal and bridging oxygen in LPS binder respectively and a peak at 532.9 eV was assigned to the C═O group in PVP.

On the prepared electrodes, satellite features were no longer noticeable, due to the strong intensity of the LPS related doublet in the Si 2*p* region. In case of GS, a main Si 2*p* peak around 103 eV was evident but the XPS shake-up satellite feature corresponding to carbon-silicon bonding in the Si 2*p* region around 108.3 eV was missing (Fig. S1a). This could be due to small intensity of the main Si 2*p* peak, its satellite features were probably lost in the noise. Additionally, XPS peak at 400.4 eV corresponding to N 1*s* was detected in GS-2 powder and its electrode with LPS binder, which was indicative of the presence of PVP in the coated samples.

Overall, the XPS results suggest that SiO_x moieties had bonded to graphite as evident from C—Si signal. However, it failed to determine the specific sites where these modifications had taken place. In addition, SiO_x coatings may also contain PVP as indicated by N 1*s* XPS spectra. Further insights into the structure of SiO_x coatings and the presence of PVP was affirmed by TERS results discussed later. These results were also consistent with the report by Kim et al. [27], where they found the role of amphiphile such as PVP to be crucial in coating basal planes of graphite. In this work they emphasized that in the absence of PVP, islands can form at the edges of graphite because of their high surface energy leading to excessive silica growth at this particular site.

To determine the thermal stability, TGA was performed for graphite, coated graphite and PVP samples as depicted in Fig. 1d. All the graphite samples were stable until 700 °C. The coated graphite samples showed a minor weight loss of about 0.7–0.8 % after 350 °C. This was in contrast with graphite, where no such weight loss was observed in this region. This indicated the presence of surface groups or a thin coating on coated graphite, which would decompose in this temperature region. PVP showed a steady weight loss of 10 % until 380 °C. At around 400 °C, it decomposed rapidly due to disintegration of its polymeric chains as depicted in the inset [32]. As evident, coated graphite samples did not contain any loosely bonded PVP as no weight loss was observed in the region corresponding to PVP. GS-2 exhibited slightly higher weight loss as compared to GS which could be due to thick coating or large number of surface groups arising from two times TEOS concentration. On the contrary, GS-5 (5 times TEOS), exhibited slightly lower weight loss as compared to GS-2.

3.2. Electrochemical performance

As a first step, coated graphite samples prepared with different concentrations of TEOS were studied in combination with LPS binder. The first few cycles were operated at low current rates (0.1C and 0.2C) to accomplish the formation of SEI, followed by a long-term cycling at 1C. The discharge capacity vs. cycle number plot is shown in the SI, Fig. S2. The GS electrode exhibited the most stable electrochemical performance as compared to the graphite and coated graphite samples prepared using higher TEOS concentrations (GS-2, GS-5). The high concentrations of TEOS led to thicker SiO_x coating as also observed in the TGA (Fig. 1d), thereby reducing the electronic conductivity as well as Li^+ ion diffusion in the material. Therefore, GS sample was used for all further studies in this work and was compared against graphite electrodes.

A total of six binders were studied with graphite (G) and coated graphite (GS). Firstly, graphite was tested with three IAB (LHPO, LPS and SMS). For reference, three well-known organic binders (PVDF, CMC, CMC-SBR) were also tested as they are widely reported with graphite anode in the literature [9,33–35]. The cells were first discharged until 0.0 V and then charged until 3.0 V at 0.1C. During the discharge process, Li^+ ions are intercalated in the graphite lattice to form LiC_6. In the first discharge process, SEI is formed on the graphite surface as indicated by the hump at about 0.6 V resulting in irreversible capacity loss from the electrochemical reduction of electrolyte [36]. The first five cycles of different systems are displayed in the SI, Figs. S3, and S4. In the subsequent cycles, the discharge profile dropped down smoothly to about 0.2 V followed by a low voltage plateau attributed to lithium intercalation/deintercalation in graphite [3,36].

3.2.1. Pristine graphite

The 2nd cycle of graphite (G) and the rate capability tests with different binders are illustrated in Fig. 2a and c respectively. The cells were cycled at different C-rates from 0.1C to 1C for 20 cycles each followed by a further 5 cycles back at 0.1C. At 0.1C, the 2nd discharge capacities (reversible capacity) of graphite obtained with different IAB were 366 (LHPO), 362 (LPS) and 371 (SMS) $mAhg^{-1}$. In contrast, reference binders (PVDF and CMC-SBR) based graphite electrodes fetched higher reversible capacities of 382 $mAhg^{-1}$ & 375 $mAhg^{-1}$, but their capacities declined to <100 $mAhg^{-1}$ within 20 cycles at 1C. Comparatively, IAB-based electrodes delivered more than double the capacities delivered by the reference-binder based electrodes. All the IAB-based electrodes also seemed to recover their capacities efficiently with a CR of >90 % after 65 cycles with the highest observed for G-LHPO (99 %).

However, CR with reference binders (PVDF and CMC) was found to be lower (~85 %) except for CMC-SBR (94 %). The interactions between graphite and PVDF are weak, arising mainly due to physisorption and/or oxygen bonding. This often leads to poor CR at higher C-rates [37,38]. In contrast, CMC-SBR adheres strongly with anode layer and current collector as compared to CMC, leading to better electrical contact with current collector [39]. SBR as an elastomer also helps to improve flexibility and to endure volume changes during charge-discharge process [40].

Clearly, the IAB outperformed all the reference binders and displayed enhanced electrochemical performance. This motivated us to test these binders at 1C for longer cycles as shown in Fig. 2e. The cells were first operated at low rates (0.1C and 0.2C) for few cycles and then at 1C. In most cases, the capacity first reduced steeply and then stabilized at 1C. The CR was therefore calculated with respect to capacity at 50th cycle (after stabilization). During cycling at 1C, most of these systems including IAB showed steep decline in their capacities. The CR trend of graphite with different binders was observed to be (CMC-SBR) > CMC > PVDF > IAB.

G-(CMC-SBR) electrode displayed the highest average capacity (270 $mAhg^{-1}$) with a CR of 92 % after 400 cycles which, however, decayed to 64 % in next 100 cycles. G-CMC and G-PVDF electrodes showed a CR of 72 % and 52 % respectively after 400 cycles. CMC is known to act as a thickener which helps to achieve the right viscosity for the coating and SBR due to its higher flexibility enhances the adhesion force between film and the current collector [41]. Therefore, combining CMC and SBR helped to achieve stable electrochemical performance even at 1C. The poor cyclic performance of G-PVDF electrode was also in line with its weak binding abilities causing delamination and electrode cracking during cycling as also seen in the SI, Fig. S6 [5]. Also, at high C-rates PVDF does not support fast intercalation of Li^+ ions due to its poor ionic conductivity which often causes lithium deposition on graphite surfaces leading to safety concerns [12].

In the case of IAB, graphite electrodes with LPS and SMS binders suffered from poor cyclic stability with a CR of only 30 % after 500 cycles at 1C. The capacity of G-LHPO electrode first reduced abruptly to 60 $mAhg^{-1}$ and then gradually stabilized to an average of 120 $mAhg^{-1}$. The poor performance of graphite with IAB at 1C could be attributed to the insufficient bonding between graphite and IAB which eventually led to capacity fading. As discussed earlier, these binders tend to form chemical bonds with functional groups present on the surface of active material during aqueous processing and drying. The probability of such favourable interactions is limited in the case of graphite due to lack of surface groups in graphite.

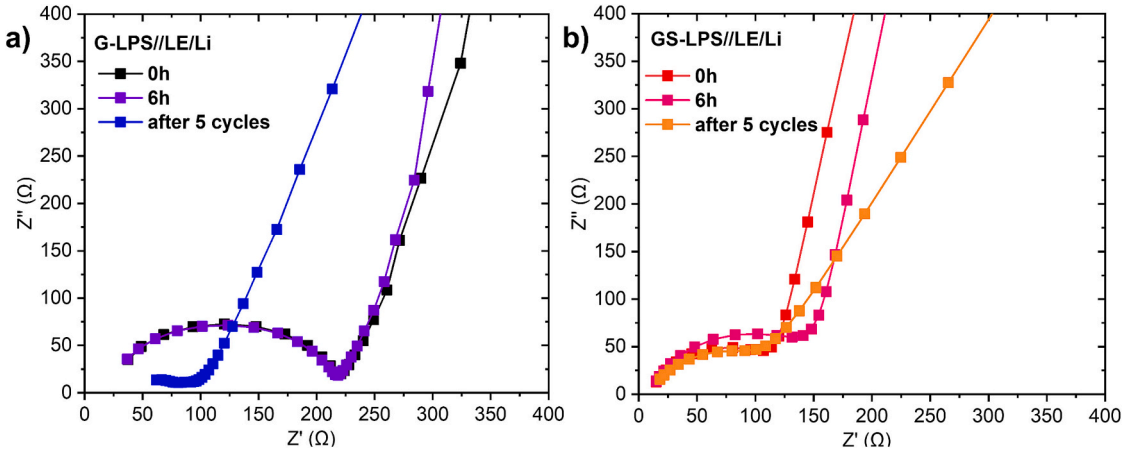

Fig. 3. Nyquist plots of graphite (G) and coated graphite (GS) at 0 h, 6 h and after 5 cycles at 0.1C a) G-LPS. b) GS-LPS. The cell configuration is graphite-LPS//liquid electrolyte (LE)//Li.

3.2.2. *Coated graphite*

To investigate the influence of surface coating on electrochemical performance, coated graphite (GS) was studied with IAB. The 2nd discharge-charge profiles of GS with LHPO, LPS and SMS binders (Fig. 2b) did not show any noticeable change in (de-)lithiation potential as compared to graphite, indicating that these coatings did not hinder the lithiation of graphite. However, the initial Coulombic efficiency (ICE) of GS got reduced by 5–10 %, probably due to irreversible Li^+ ion trapping on SiO_x surface groups. Rate capability tests for GS were performed similar to graphite and are shown in Fig. 2d. At 0.1C, the reversible capacities of GS with LHPO, LPS and SMS binders were observed to be 390, 344 and 363 $mAhg^{-1}$ respectively. Significant improvements were observed at 1C, highest capacity (356 $mAhg^{-1}$) was obtained for GS-LHPO electrode, corresponding to an improvement of 23 % as compared to G-LHPO electrode. With SMS binder, the capacity of GS was almost doubled (97 % increase) whereas with LPS binder, it showed an increase of 15 % as compared to their graphite electrodes.

The observed CR of GS was >95 % for all IAB after 65 cycles. These drastic improvements in the electrochemical performances for the case of coated graphite with IAB agreed well with our hypothesis, that the SiO_x surface coatings on graphite can provide adequate chemical bonding with IAB, which could enable stable electrochemical cycling.

Owing to the immense improvement in electrochemical performance of GS with IAB, it was also tested at 1C for prolonged cycling and compared against graphite electrodes as shown in Fig. 2e. All the cells were first operated at low C-rates for few cycles and then high current corresponding to 1C were applied. GS showed an outstanding improvement in its capacity and cyclic stability with LPS and SMS binders. It maintained a capacity >310 $mAhg^{-1}$ for both LPS and SMS binders. After 500 cycles at 1C, both GS-LPS and GS-SMS electrodes displayed almost negligible loss in their capacity and showed a very high CR of ~100 % and 98 % respectively. This was almost three times superior to graphite where only 30 % of CR was noted at this stage with these IAB. GS-LPS electrode showed an excellent cyclic stability (CR >95 %) until 800 cycles, followed by a minor decline in its capacity. GS-SMS electrode also displayed similar trend with a CR of >93 % until 800 cycles followed by a steady drop. With LHPO binder, GS showcased ~70 % improvement (120 $mAhg^{-1}$ to 205 $mAhg^{-1}$) in its average capacity at 1C but its CR after 500 cycles was only 53 %. This suggests that SiO_x coatings do not have high bonding affinity with phosphate-based binders and hint towards the presence of favoured chemical interaction between SiO_x coating and silicate based IAB. Besides, nano-SiO_2 is hydrophilic in nature, due to the presence of hydroxyl groups on it [42] as was confirmed by an XPS signal at 531.9 eV in O 1*s* region (Fig. S1d). The SiO_x coating on graphite facilitated the formulation of uniform slurry and also improved the coating quality with IAB (Fig. S7). The superior electrochemical performance with IAB at high C-rate could also be due to their intrinsic ionic conductivity [14], which aids Li^+ ion diffusion particularly in the case of electrolyte drying during long cycling [43].

In order to investigate the effect of SiO_x coating with organic binder, GS was tested with CMC but the cyclic performance deteriorated rapidly (Fig. S8). This was probably due to insufficient interactions between the coated layer and CMC binder. The findings further validated that these coatings were only helpful with silicate-based binders. Further insights on morphological and microstructural investigations by TEM and TERS are detailed in Section 3.3.

3.2.3. *Electrochemical impedance spectroscopy (EIS)*

EIS was carried out for graphite (G) and coated graphite (GS) electrodes with LPS binder at three separate instances, 0 h (immediately after cell fabrication), after 6 h and after 5 cycles. The EIS spectra are compared in Fig. 3. The Nyquist plots of graphite half cells displayed a semicircle with an intercept on x-axis (Z′) indicating charge transfer resistance (R_{ct}) followed by a Warburg impedance observed as a straight line [44]. The R_{ct} was found to be lower for coated graphite, probably due to better electrode wettability with the electrolyte and improved interfacial contact with LPS binder. The impedance of graphite was ~220 Ω, which remained unchanged with time. However, a slight increase in impedance from 115 Ω (0 h) to 140 Ω (6 h) was observed for coated graphite (GS-LPS).

After 5 cycles, the impedances reduced for both cells (G-LPS: 96 Ω, GS-LPS: 108 Ω) due to the formation of SEI on graphite surface leading to improved Li^+ ion diffusion kinetics. The Li^+ ion diffusion through SEI is the rate determining step for Li^+ ion transfer in graphite anode [44,45]. The kinetics is largely dependent on SEI composition, which is significantly influenced by choice of binder. It can therefore be speculated that graphite and coated graphite would have different SEI composition with each binder which needs further investigation. However, it was evident that the SEI and surface chemistry of the inorganic binders did not impair the diffusion of Li^+ ions through it.

3.2.4. *5 wt% binders*

The optimization of electrode composition plays a vital role in processing high quality slurry and improve electrochemical performance. Binders comprise of a small portion (<5 wt%) of a battery electrode in commercial batteries [46]. Therefore, electrochemical performance was also evaluated with 5 and 2.5 wt% binders and is shown in Figs. S9 and S10 and summarized in Tables S4 and S5 in the SI. GS performed remarkably well even with 5 wt% of silicate-based IAB. Capacities >260 $mAhg^{-1}$ were obtained with LPS and SMS binders at 1C with negligible capacity loss until 500 cycles. GS-SMS emerged out to be most stable

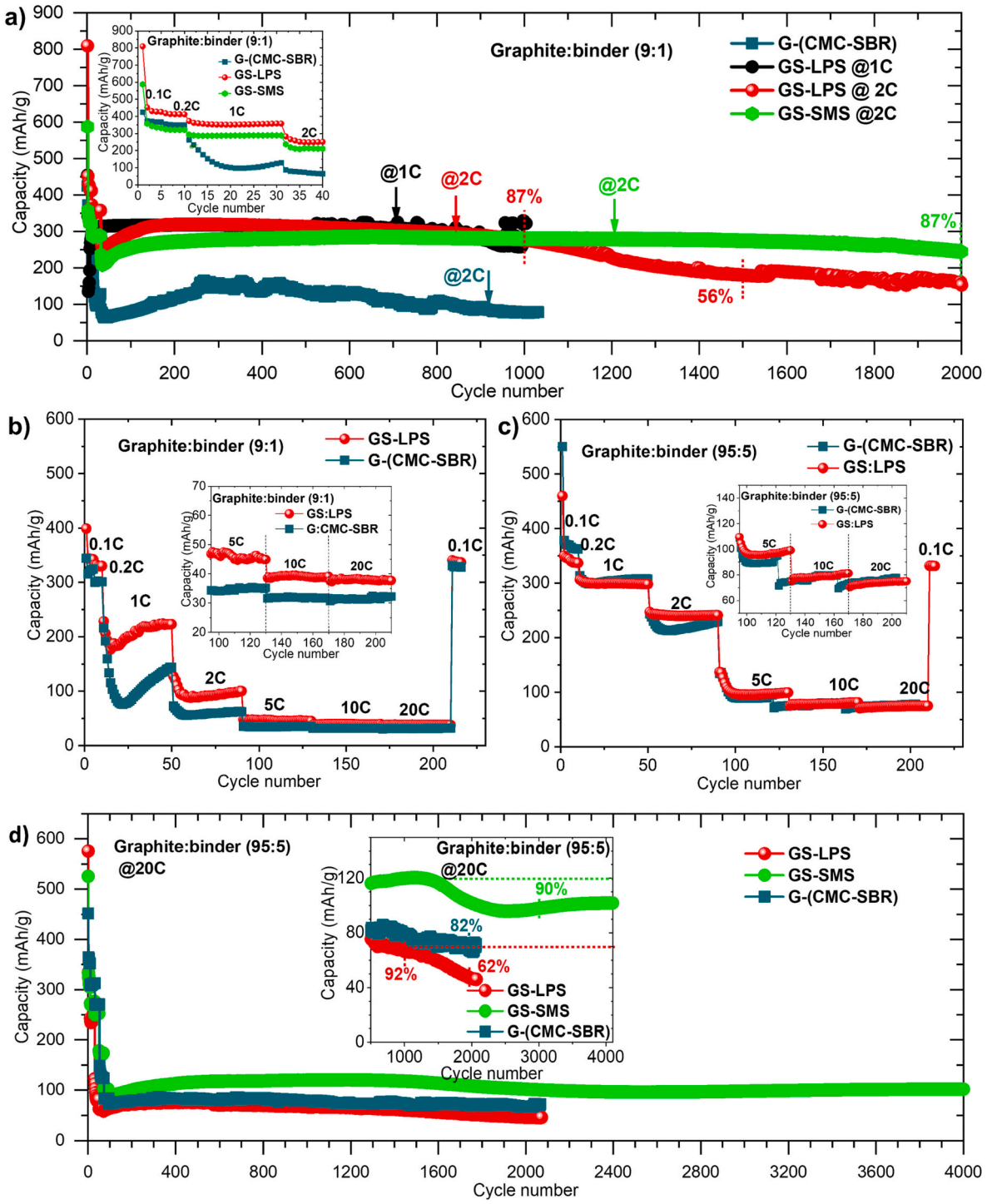

Fig. 4. High rate test. a) Cyclic performance of GS-LPS and G-(CMC-SBR) at 2C. b) Rate capability of GS-LPS and G-(CMC-SBR) with 10 wt% binder. c) Rate capability of GS-LPS, G-CMC and G-(CMC-SBR) with 5 wt% binder. d) Cycling performance of GS-LPS, GS-SMS and G-(CMC-SBR) at 20C. The SEM image of cycled electrode of GS:SMS is shown in Fig. S11. The electrochemical performance is summarized in the Tables S6–S9 in the SI.

system with CR of ~95 % after 1000 cycles at 1C. Among the reference binders, G-CMC electrodes exhibited the highest CR of 57 % after 500 cycles at 1C.

3.2.5. *High-rate tests*

One of the major challenges in application of graphite in LIBs for electric vehicles is fast charging time and difficulty in sustaining longer cycle life [47]. Therefore, high-rate cycling tests were performed. The stable cyclic performance at 1C, allowed to further test these samples up to 20C in a systematic manner.

In the first test, GS was cycled with 10 wt% of LPS and SMS binders at 2C for 2000 cycles. The key aspect in high-rate cycling is the formation of a stable SEI. Therefore, SEI of these systems were allowed to stabilize by cycling at lower C-rates for 30 cycles. The current was increased in a stepwise manner up to 2C as depicted in the inset (Fig. 4a). Capacity of ~320 $mAhg^{-1}$ was obtained at 2C for GS-LPS electrode which overlaps with its performance at 1C (also shown in Fig. 2e), delivering similar capacity at double C-rate. The system retained a capacity of 87 % after

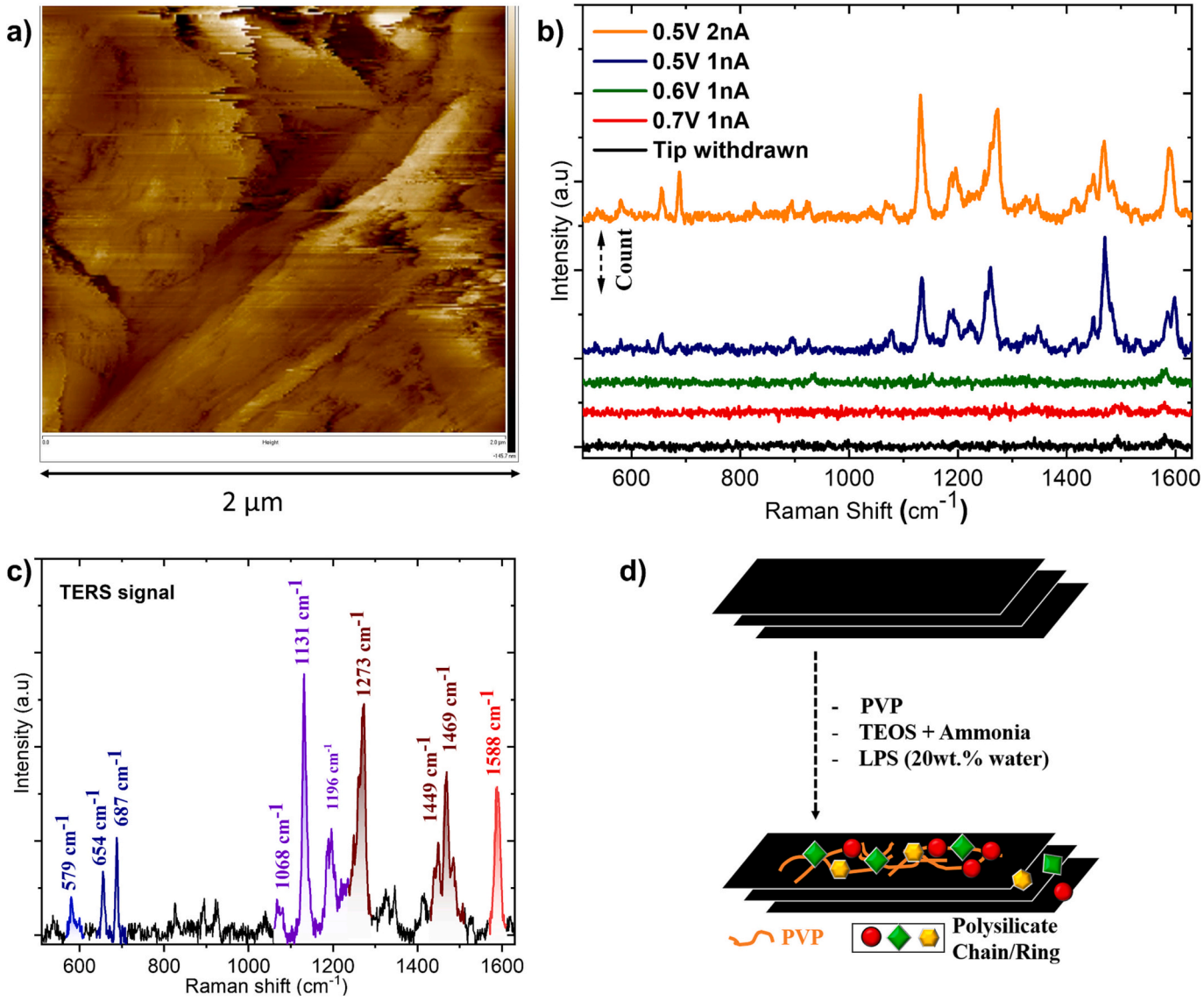

Fig. 5. TERS of coated graphite (GS). a) STM image b) TERS spectra c) TERS spectra at 2 nA & 0.5 V bias d) Schematic of coated graphite along with LPS binder (GS-LPS).

1000 cycles at 2C. After this, the capacity faded gradually, retaining more than half of its capacity after 2000 cycles. GS-SMS electrode showed an average capacity of 279 $mAhg^{-1}$ at 2C and retained ~87 % of its capacity after 2000 cycles.

The SEI properties are significantly affected by cell conditions like operation temperature, state of charge and current rate. Cycling at higher current rates accelerates the growth of SEI and causes capacity loss [48,49]. Higher current rates in graphite are also susceptible to lithium plating and, hence, are a safety issue in case of inefficient SEI [50]. Therefore, low current rates should initially be applied to form a stable SEI in first few cycles. For a comparison, G-(CMC-SBR) electrode was also cycled at 2C but it could only yield nearly half of the capacity as showcased by GS-LPS electrode.

In the second experiment, high-rate capability tests were performed by sequentially increasing current up to 20C. GS-LPS and G-(CMC-SBR) electrodes were cycled from 0.1C to 20C for 40 cycles at each C-rate with 10 wt% and 5 wt% binder composition. The capacity vs. cycle number plots are compared in Fig. 4b for 10 wt% binder and Fig. 4c for 5 wt% binder with magnified images in respective insets. GS-LPS electrode outperformed G-(CMC-SBR) based electrodes at all C-rates. At 20C, GS-LPS electrode delivered a capacity of 38 $mAhg^{-1}$ with 10 wt% binder but only 31 mAh/g in the case of G-(CMC-SBR) electrode.

For 5 wt% binder, although considerable difference was not observed in capacities of the two at high rates (5C-20C) but G-(CMC-SBR) electrode failed to recover after cycling at 20C. In contrast, GS-LPS electrode exhibited a CR of 94 % even after cycling at 20C owing to the high bonding strength between GS and LPS.

In third cycling test, prolonged cycling (>4000 cycles) was performed for GS with 5 wt% of LPS and SMS binders at 20C as shown in Fig. 4d. GS-LPS electrode showed an average capacity of ~71 $mAhg^{-1}$ followed by a gradual decline to 92 % capacity after 1000 cycles. In next 1000 cycles, ~64 % capacity could still be retained. Comparatively, in GS-SMS electrode a higher capacity (~120 $mAhg^{-1}$) was obtained with a very stable cyclic performance until 1500 cycles. After this only <10 % capacity loss was observed during cycling until 4000 cycles. The SEM analysis of this cycled electrode was performed and is shown in Fig. S11. The morphological and structural integrity of graphite remained unchanged and no major changes were observed in the morphology. For a comparison, G-(CMC-SBR) electrode was also tested at 20C which showed 35 % lower capacity (71 mAg^{-1}) and stability up to 2000 cycles. The high-rate performance is summarized in the SI, Tables S6–S9.

The outstanding performance of IAB particularly SMS even at high C-

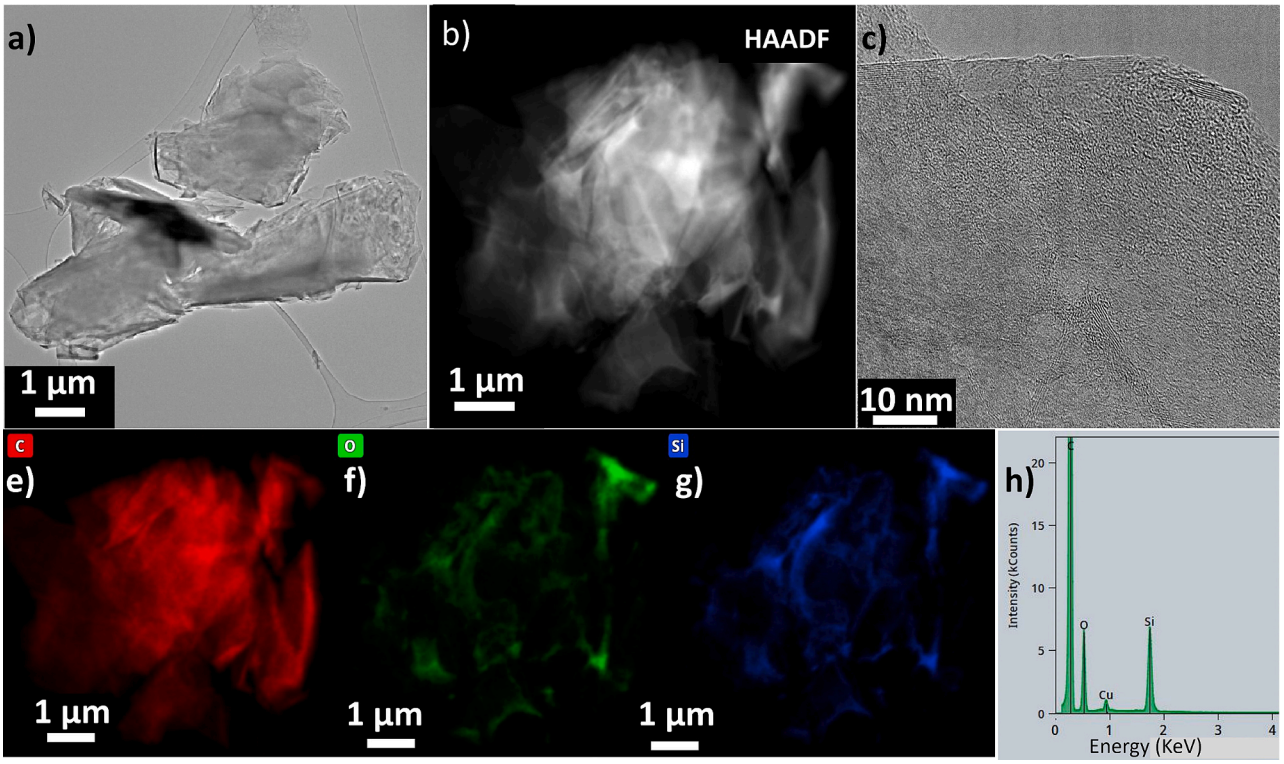

Fig. 6. TEM, mapping and EDX spectra of GS-LPS pristine electrode. a) TEM image b) HAADF image c) corresponding HRTEM image d)–f) Elemental mapping of carbon, oxygen and silicon g) EDX spectra of GS-LPS.

rates could also be ascribed to their much higher adhesion strength as compared to reference binders. SMS binder showed an adhesion strength of 9 N as compared to only 1.6 N and 4.2 N for PVDF and CMC respectively (Fig. S12). Moreover, SMS was also reported to maintain Young's modulus of >50 GPa and does not soften even in presence of liquid electrolyte unlike organic binders such as PVDF [51]. This report also claimed that SMS formed a lithium-conducting binder by Li-Na cation exchange via in situ process during cycling in LIB. The superior performance of coated graphite could also be explained from TEM analysis which revealed the presence of binder coating on graphite particles preventing microcracking and pulverization during cycling at high C-rates.

3.3. Surface investigations

3.3.1. Tip enhanced Raman spectroscopy (TERS)

The physicochemical characterizations by XPS (Fig. 1c) could only confirm that silicon is bonded to graphitic carbon atoms along with PVP in the coated graphite. It however, failed to clarify the structural organization of coated graphite and its chemical interaction with IAB. The Raman spectra presented in Fig. 1b could only capture prominent bands of graphite and also failed to confirm the presence of SiO_x coating on the graphite surface. Therefore, TERS measurements were performed. It combines the chemical sensitivity of surface-enhanced Raman spectroscopy (SERS) with high spatial resolution of scanning probe microscopy and enables chemical imaging of surfaces at the nanometer length-scale. To elucidate the organizational correlation between silicon oxide coating and binder, TERS technique was utilized.

Fig. 5a and b show STM image and TERS spectra obtained at different tunneling current and applied bias voltage. When the tip was far away from the surface, i.e. in withdrawn mode, no Raman signal (Fig. 5b) was observed. As the applied bias voltage reduced and tip was engaged TERS signal from the electrode surface emerged revealing physical and chemical affinity among graphite surface, silicon oxide coating and LPS binder. A close inspection of the TERS spectra recorded at 2 nA tunneling current and 0.5 V bias voltage is presented in Fig. 5c and all the relevant bands are highlighted. Table S10 in the SI provides the assigned Raman bands corresponding to specific vibration present in the GS-LPS electrode. The band centered at 1588 cm^{-1} comes from G-band [52], suggesting the region probed by the TERS was basal plane of graphite. The broad band ~1440–1490 cm^{-1} is assigned as —CH_2 scissor vibration [53,54]. The Raman band centered at ~1273 cm^{-1} is assigned to both —CH_2 out of plane vibration or C—N stretching vibration [53]. The low frequency band centered at 579 cm^{-1} is attributed to N—C═O bending [54], leading to ring deformation type vibration.

The abovementioned Raman fingerprints strongly suggest that a thin film of PVP is present on top of graphite basal plane. The Raman bands centered at 1196, 1131 and 1068 cm^{-1} are associated with Si—O symmetric stretching [55–57] which are present in polysilicate chain whereas 687 and 654 cm^{-1} bands are assigned to Si—O symmetric breathing present in Si—O ring-like structure [55,57,58]. Previous studies of silicate glasses have demonstrated that silicon-oxygen tetrahedra with various numbers of bridging oxygen atoms are the fundamental structural blocks in polysilicate materials. The silicon-oxygen tetrahedra are called Q^n units, where n (n = 0–4) is the number of bridging oxygen atoms per SiO_4 tetrahedron [55,56]. Broad Raman bands in the region 800–1200 cm^{-1} are a signature of alkali silicate amorphous glasses, in which ~800 cm^{-1} is assigned to the isolated SiO_4 tetrahedron (Q^0). In TERS spectra, the absence of any band at 800 cm^{-1} points to a silicate structure containing interlinked, polymeric SiO_4 tetrahedra rather than isolated SiO_4 tetrahedra (Q^0). The bands centered at 1196, 1131 and 1068 cm^{-1} can be ascribed as Q^4, Q^3 and Q^2 types of SiO_4 tetrahedron, reinforcing the presence of previously mentioned polymeric silicate moiety. The narrow Raman bands pointed towards a highly ordered silicate structure. Polysilicate can also form two, three or four-membered rings resembling as a planer mosaic structure. Raman bands centered at 687 and 654 cm^{-1} are arising from two and three-membered ring-like structures [58,59].

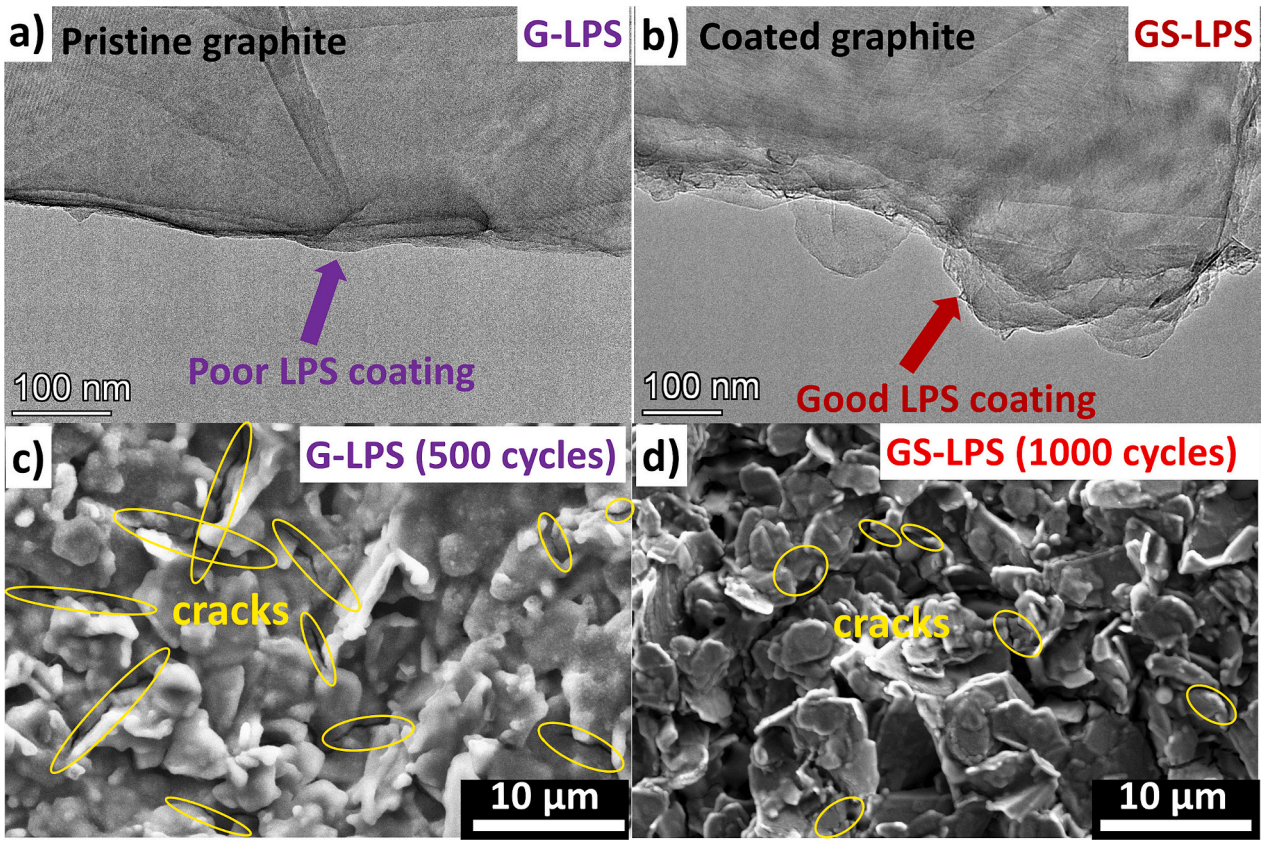

Fig. 7. Morphological characterizations of graphite (G) and coated-graphite (GS) electrodes with 10 wt% LPS binder: TEM images before cycling; a) Graphite electrode b) Coated-graphite electrode. SEM image of cycled-electrodes of; a) Graphite after 500 cycles at 1C, b) Coated-graphite after 1000 cycles at 1C. The cycled cells were disassembled inside the glove box and the electrodes were washed with DMC to remove excess electrolyte and then dried at 60 °C before SEM measurement.

In conclusion, TERS revealed that GS-LPS electrodes have a very intricate synergy. Graphite was coated with PVP which assisted the coating of silicon oxide layer. The LPS binder combines with this silicon oxide to form polysilicate chain, two or three-membered ring-like structures which exhibit local ordering. A schematic of this coordinated structural and chemical-driven harmony is presented in Fig. 5d. Perhaps this interaction of these chemical and structural arrangements of surface coating and binder enhanced the electrochemical performance in the GS-LPS electrode.

3.3.2. Microstructural investigations

Electron microscopy (SEM and TEM) analysis were carried out to examine the morphology, ascertain the nature of coating and investigate structural changes after cycling. Firstly, TEM analysis was carried out for graphite and coated graphite (GS and GS-5) powder as portrayed in the SI, Figs. S13–S15. The TEM images exhibited a flake like morphology of graphite without any noticeable structural or morphological change after coating. Sharp peaks corresponding to carbon and oxygen were observed in the EDX spectra. Additional copper peak was a contribution from the TEM grid. GS showed a silicon signal arising from the SiO_x coating, but it was disguised due to poor signal to noise ratio (Fig. S14). This however was more evident in GS-5 which had thicker SiO_x coating (Fig. S15). The elemental mapping from TEM-EDX confirmed that silicon and oxygen were uniformly distributed in both GS and GS-5 powder samples which affirmed the uniform coating of graphite. These results were also consistent with TERS signals arising from different surfaces like basal planes and edges of graphite, confirming uniform coating on graphite.

To investigate the nature of coatings, the powder was scrapped from pristine electrodes of G-LPS and GS-LPS and TEM analysis was carried out, as shown in Figs. 6 and S16 in the SI. Micrometric graphite with flake like morphology was observed featuring highly crystalline regions of graphite along with the edges (Fig. 6c).

The elemental mapping of carbon, oxygen and silicon was observed to be uniform throughout the sampled area. Mapping of Si intensity confirmed that LPS binder was homogenously distributed over the electrode. The EDX spectra displayed sharp peaks of carbon, oxygen and silicon. The silicon signal was more intense in the electrode as observed in the case of powder samples due to contribution from the LPS binder.

Fig. 7a and b show TEM images of pristine electrodes of G and GS with LPS binder. The powders from respective electrodes were scrapped off and analysed under a TEM. GS-LPS electrode showed a layer of binder coated over graphite particles, probably due to enhanced silicate (—O—Si—O—) bonding between GS and LPS binder. This binder layer may also have acted as a protective layer during long cycling, avoiding the formation of microcracks and electrolyte decomposition at high C-rates. Often these cracks create fresh and reactive surfaces leading to electrolyte decomposition and thereby contributing to capacity fading. The binder layer was observed to be non-uniform perhaps due to higher binder content (10 wt%) which would need further optimization of electrode composition and slurry formulation method to achieve thin and uniform binder layer over GS. This protective layer of binder could be more optimal and uniform with 5 wt% binder content. No such protective layer was observed in the case of G-LPS, which also corroborates well with its drastic loss in capacity.

To further comprehend their cyclic behaviour, SEM was carried out for cycled electrodes of G-LPS and GS-LPS. Fig. 7c shows SEM of G-LPS electrode after 500 cycles at 1C. The graphite flakes looked agglomerated and coalesced. Also, there was excessive electrolyte decomposition as observed from thick SEI blanketed over graphite particles. Several

cracks were detected on the graphite surface which could act as a site for electrolyte decomposition. The SEM of the pristine electrodes are shown in Figs. S17 and S18 for a comparison. However, the morphology of GS-LPS after 1000 cycles at 1C remained unchanged with obvious flake like morphology and minimum cracks (Fig. 7d).

These results assert the significance of SiO_x coating on graphite for usage with silicate-based IAB. It is well known that the binder plays a significant role in SEI formation which is crucial in deciding electrochemical performance [60]. The nature of SEI formed in both cases would be different, which needs further investigation.

4. Conclusions and outlook

In conclusion, to improve the electrochemical performance of graphite anode, SiO_x surface coatings of graphite were carried out using a wet chemical process. These coatings were found to be highly effective to improve electrochemical performance of graphite with IAB. The coated graphite worked exceptionally well with silicate-based IAB due to improved bonding between coated layer and these binders leading to stable cycling even at high C-rates. It delivered a high capacity of >315 $mAhg^{-1}$ at 2C with LPS binder, stable for over 1000 cycles with a capacity retention of 87 %. At 20C, combination of coated graphite and SMS binder achieved a capacity of ~120 $mAhg^{-1}$ and a capacity retention of >90 % after 4000 cycles, making it the most stable and reliable combination. The TEM results revealed that these binders tend to form a surface protective layer on coated graphite leading to stable cyclic performance unlike pristine graphite. The nature of coatings was studied by TERS, XPS and electron microscopy. These SiO_x coatings were however not very successful with phosphate based IAB investigated here. To improve electrochemical performance with phosphate-based IAB, surface modification of graphite with phosphate-based coatings such as Li_3PO_4 would be necessary. Overall, this surface coating strategy could also be extended to improve performances of different electrode materials by employing a suitable inorganic binder and surface coating on active material.

Authors' declaration

I, Shivam Trivedi, on the behalf of all the co-authors state that all the co-authors have contributed and approved this manuscript. There are no conflict of interest or financial interests associated with this manuscript.

CRediT authorship contribution statement

M. A. Reddy: idea & conceptualizing; **S. Trivedi**: planning, conceptualization, investigation, formal analysis, original draft; **S. Dinda**: investigation-Raman spectroscopy & TERS, formal analysis, writing, review & editing; **Y. Tang**: investigation-TEM; **S. Fuchs**: investigation-XPS, writing; **V. Pamidi**: investigation, review & editing; **H. S. Stein**: resources; **M. Fichtner**: resources, supervision, review & editing, project administration & funding acquisition.

Declaration of competing interest

The authors declare that they have no known competing financial interests or personal relationships that could have appeared to influence the work reported in this paper.

Data availability

Data will be made available on request.

Acknowledgments

This work contributes to the research performed at CELEST (Center for Electrochemical Energy Storage Ulm-Karlsruhe) and was funded by the German Research Foundation (DFG) under project ID 390874152 (POLiS Cluster of Excellence, EXC 2154). The authors thank Prof. Christian Kübel for the TEM facility and Mr. Ruochen Xu for his help in the measurement of adhesion strength. ST acknowledges Mr. Ananyo Roy for proofreading the draft.

Appendix A. Supplementary data

Supplementary data to this article can be found online at https://doi.org/10.1016/j.est.2023.109210.

References

[1] S. Trivedi, K. Lobo, H.S.S. Ramakrishna Matte, Synthesis, properties, and applications of graphene, in: Fundamentals and Sensing Applications of 2D Materials, Elsevier, 2019, pp. 25–90, https://doi.org/10.1016/B978-0-08-102577-2.00003-8.
[2] H. Zhang, Y. Yang, D. Ren, L. Wang, X. He, Graphite as anode materials: fundamental mechanism, recent progress and advances, Energy Storage Mater. 36 (2021) 147–170, https://doi.org/10.1016/j.ensm.2020.12.027.
[3] J. Asenbauer, T. Eisenmann, M. Kuenzel, A. Kazzazi, Z. Chen, D. Bresser, The success story of graphite as a lithium-ion anode material – fundamentals, remaining challenges, and recent developments including silicon (oxide) composites, Sustain. Energy Fuels 4 (2020) 5387–5416, https://doi.org/10.1039/D0SE00175A.
[4] S.L. Chou, Y. Pan, J.Z. Wang, H.K. Liu, S.X. Dou, Small things make a big difference: binder effects on the performance of Li and Na batteries, Phys. Chem. Chem. Phys. 16 (2014) 20347–20359, https://doi.org/10.1039/c4cp02475c.
[5] D. Bresser, D. Buchholz, A. Moretti, A. Varzi, S. Passerini, Alternative binders for sustainable electrochemical energy storage – the transition to aqueous electrode processing and bio-derived polymers, Energ. Environ. Sci. 11 (2018), https://doi.org/10.1039/C8EE00640G.
[6] D.E. Malek, L.A. Malley, T.W. Slone, G.S. Elliott, G.L. Kennedy, W. Mellert, K. Deckardt, C. Gembardt, B. Hildebrand, S.R. Murphy, D.B. Bower, G.A. Wright, Repeated dose toxicity study (28 days) in rats and mice with N-methylpyrrolidone (NMP), Drug Chem. Toxicol. 20 (1997) 63–77, https://doi.org/10.3109/01480549709011079.
[7] J. Shim, Electrochemical analysis for cycle performance and capacity fading of a lithium-ion battery cycled at elevated temperature, J. Power Sources 112 (2002) 222–230, https://doi.org/10.1016/S0378-7753(02)00363-4.
[8] J.T. Li, Z.Y. Wu, Y.Q. Lu, Y. Zhou, Q.S. Huang, L. Huang, S.-G. Sun, Water soluble binder, an electrochemical performance booster for electrode materials with high energy density, Adv. Energy Mater. 7 (2017), https://doi.org/10.1002/aenm.201701185.
[9] J.-H. Lee, S. Lee, U. Paik, Y.-M. Choi, Aqueous processing of natural graphite particulates for lithium-ion battery anodes and their electrochemical performance, J. Power Sources 147 (2005) 249–255, https://doi.org/10.1016/j.jpowsour.2005.01.022.
[10] J.-H. Lee, U. Paik, V.A. Hackley, Y.-M. Choi, Effect of carboxymethyl cellulose on aqueous processing of natural graphite negative electrodes and their electrochemical performance for lithium batteries, J. Electrochem. Soc. 152 (2005), https://doi.org/10.1149/1.1979214.
[11] H. Buqa, M. Holzapfel, F. Krumeich, C. Veit, P. Novák, Study of styrene butadiene rubber and sodium methyl cellulose as binder for negative electrodes in lithium-ion batteries, J. Power Sources 161 (2006) 617–622, https://doi.org/10.1016/j.jpowsour.2006.03.073.
[12] F. Zou, A. Manthiram, A review of the design of advanced binders for high-performance batteries, Adv. Energy Mater. 10 (2020) 2002508, https://doi.org/10.1002/aenm.202002508.
[13] L. Qiu, Z. Shao, M. Yang, W. Wang, F. Wang, J. Wan, J. Wang, Y. Bi, H. Duan, Study on effects of carboxymethyl cellulose lithium (CMC-Li) synthesis and electrospinning on high-rate lithium-ion batteries, Cellulose. 21 (2014) 615–626, https://doi.org/10.1007/s10570-013-0108-z.
[14] S. Trivedi, V. Pamidi, M. Fichtner, M. Anji Reddy, Ionically conducting inorganic binders: a paradigm shift in electrochemical energy storage, Green Chem. 24 (2022) 5620–5631, https://doi.org/10.1039/D2GC01389D.
[15] C. Wei, M.N. Obrovac, Inorganic compounds as binders for Si-alloy anodes, J. Electrochem. Soc. 168 (2021), 020505, https://doi.org/10.1149/1945-7111/abdc74.
[16] A. Mauger, C. Julien, Surface modifications of electrode materials for lithium-ion batteries: status and trends, Ionics (Kiel). 20 (2014) 751–787, https://doi.org/10.1007/s11581-014-1131-2.
[17] S.F. Lux, T. Placke, C. Engelhardt, S. Nowak, P. Bieker, K.-E. Wirth, S. Passerini, M. Winter, H.-W. Meyer, Enhanced electrochemical performance of graphite anodes for lithium-ion batteries by dry coating with hydrophobic fumed silica, J. Electrochem. Soc. 159 (2012) A1849–A1855, https://doi.org/10.1149/2.070211jes.
[18] H. Nozaki, K. Nagaoka, K. Hoshi, N. Ohta, M. Inagaki, Carbon-coated graphite for anode of lithium-ion rechargeable batteries: carbon coating conditions and precursors, J. Power Sources 194 (2009) 486–493, https://doi.org/10.1016/j.jpowsour.2009.05.040.

[19] M. Mancini, F. Nobili, S. Dsoke, F. D'Amico, R. Tossici, F. Croce, R. Marassi, Lithium intercalation and interfacial kinetics of composite anodes formed by oxidized graphite and copper, J. Power Sources 190 (2009) 141–148, https://doi.org/10.1016/j.jpowsour.2008.10.084.

[20] F. Nobili, M. Mancini, S. Dsoke, R. Tossici, R. Marassi, Low-temperature behavior of graphite–tin composite anodes for Li-ion batteries, J. Power Sources 195 (2010) 7090–7097, https://doi.org/10.1016/j.jpowsour.2010.05.001.

[21] J. Gao, L.J. Fu, H.P. Zhang, L.C. Yang, Y.P. Wu, Improving electrochemical performance of graphitic carbon in PC-based electrolyte by nano-TiO2 coating, ElectrochimActa. 53 (2008) 2376–2379, https://doi.org/10.1016/j.electacta.2007.09.058.

[22] Q. Pan, K. Guo, L. Wang, S. Fang, Novel modified graphite as anode material for lithium-ion batteries, J. Electrochem. Soc. 149 (2002) A1218, https://doi.org/10.1149/1.1499499.

[23] W. Li, W. Feng, H. Huang, High-performance epoxy resin/silica coated flake graphite composites for thermal conductivity and electrical insulation, J. Mater. Sci. Mater. Electron. 27 (2016) 6364–6370, https://doi.org/10.1007/s10854-016-4571-9.

[24] Y. Cho, J. Cho, Significant improvement of $LiNi_{0.8}Co_{0.15}Al_{0.05}O_2$Cathodes at 60°C by SiO_2 dry coating for Li-ion batteries, J. Electrochem. Soc. 157 (2010) A625, https://doi.org/10.1149/1.3363852.

[25] D. Arumugam, G. Paruthimal Kalaignan, Synthesis and electrochemical characterizations of Nano-SiO2-coated LiMn2O4 cathode materials for rechargeable lithium batteries, J. Electroanal. Chem. 624 (2008) 197–204, https://doi.org/10.1016/j.jelechem.2008.09.007.

[26] Y. Yang, W. Peng, H. Guo, Z. Wang, X. Li, Y. Zhou, Y. Liu, Effects of modification on performance of natural graphite coated by SiO2 for anode of lithium-ion batteries, Trans. Nonferrous Met. Soc. Chin. 17 (2007) 1339–1342, https://doi.org/10.1016/S1003-6326(07)60273-8.

[27] Y. Kim, Y. Qian, M. Kim, J. Ju, S.-H. Baeck, S.E. Shim, A one-step process employing various amphiphiles for an electrically insulating silica coating on graphite, RSC Adv. 7 (2017) 24242–24254, https://doi.org/10.1039/C7RA03049E.

[28] H.S. Stein, A. Sanin, F. Rahmanian, B. Zhang, M. Vogler, J.K. Flowers, L. Fischer, S. Fuchs, N. Choudhary, L. Schroeder, From materials discovery to system optimization by integrating combinatorial electrochemistry and data science, Curr. Opin. Electrochem. 35 (2022), 101053, https://doi.org/10.1016/j.coelec.2022.101053.

[29] A.C. Ferrari, Raman spectroscopy of graphene and graphite: disorder, electron–phonon coupling, doping and nonadiabatic effects, Solid State Commun. 143 (2007) 47–57, https://doi.org/10.1016/j.ssc.2007.03.052.

[30] J.A. Gardella, S.A. Ferguson, R.L. Chin, $\pi^* \leftarrow \pi$ shakeup satellites for the analysis of structure and bonding in aromatic polymers by X-ray photoelectron spectroscopy, Appl. Spectrosc. 40 (1986) 224–232, https://doi.org/10.1366/0003702864509565.

[31] P.M.Th.M. van Attekum, G.K. Wertheim, Excitonic effects in core-hole screening, Phys. Rev. Lett. 43 (1979) 1896–1898, https://doi.org/10.1103/PhysRevLett.43.1896.

[32] T.H.C. Salles, C.B. Lombello, M.A. d'Ávila, Electrospinning of gelatin/poly (vinyl pyrrolidone) blends from water/acetic acid solutions, Mater. Res. 18 (2015) 509–518, https://doi.org/10.1590/1516-1439.310114.

[33] J. Drofenik, M. Gaberscek, R. Dominko, F.W. Poulsen, M. Mogensen, S. Pejovnik, J. Jamnik, Cellulose as a binding material in graphitic anodes for Li-ion batteries: a performance and degradation study, Electrochim. Acta 48 (2003) 883–889, https://doi.org/10.1016/S0013-4686(02)00784-3.

[34] C. Forestier, S. Grugeon, C. Davoisne, A. Lecocq, G. Marlair, M. Armand, L. Sannier, S. Laruelle, Graphite electrode thermal behavior and solid electrolyte interphase investigations: role of state-of-the-art binders, carbonate additives and lithium bis (fluorosulfonyl)imide salt, J. Power Sources 330 (2016) 186–194, https://doi.org/10.1016/j.jpowsour.2016.09.005.

[35] N. Lingappan, L. Kong, M. Pecht, The significance of aqueous binders in lithium-ion batteries, Renew. Sustain. Energy Rev. 147 (2021), 111227, https://doi.org/10.1016/j.rser.2021.111227.

[36] S.J. An, J. Li, C. Daniel, D. Mohanty, S. Nagpure, D.L. Wood, The state of understanding of the lithium-ion-battery graphite solid electrolyte interphase (SEI) and its relationship to formation cycling, Carbon N Y. 105 (2016) 52–76, https://doi.org/10.1016/j.carbon.2016.04.008.

[37] M. Yoo, C.W. Frank, S. Mori, Interaction of poly(vinylidene fluoride) with graphite particles. 1. Surface morphology of a composite film and its relation to processing parameters, Chem. Mater. 15 (2003) 850–861, https://doi.org/10.1021/cm0209970.

[38] M. Yoo, C.W. Frank, S. Mori, S. Yamaguchi, Effect of poly(vinylidene fluoride) binder crystallinity and graphite structure on the mechanical strength of the composite anode in a lithium ion battery, Polymer (Guildf.) 44 (2003) 4197–4204, https://doi.org/10.1016/S0032-3861(03)00364-1.

[39] R. Gordon, R. Orias, N. Willenbacher, Effect of carboxymethyl cellulose on the flow behavior of lithium-ion battery anode slurries and the electrical as well as mechanical properties of corresponding dry layers, J. Mater. Sci. 55 (2020) 15867–15881, https://doi.org/10.1007/s10853-020-05122-3.

[40] W. Wang, X. Yue, J. Meng, X. Wang, Y. Zhou, Q. Wang, Z. Fu, Comparative study of water-based LA133 and CMC/SBR binders for sulfur cathode in advanced lithium–sulfur batteries, J. Phys. Chem. C 123 (2019) 250–257, https://doi.org/10.1021/acs.jpcc.8b10736.

[41] S. Lim, S. Kim, K.H. Ahn, S.J. Lee, The effect of binders on the rheological properties and the microstructure formation of lithium-ion battery anode slurries, J. Power Sources 299 (2015) 221–230, https://doi.org/10.1016/j.jpowsour.2015.09.009.

[42] B. Xu, Q. Zhang, Preparation and properties of hydrophobically modified Nano-SiO_2 with hexadecyltrimethoxysilane, ACS Omega 6 (2021) 9764–9770, https://doi.org/10.1021/acsomega.1c00381.

[43] C. Niu, D. Liu, J.A. Lochala, C.S. Anderson, X. Cao, M.E. Gross, W. Xu, J.-G. Zhang, M.S. Whittingham, J. Xiao, J. Liu, Balancing interfacial reactions to achieve long cycle life in high-energy lithium metal batteries, Nat. Energy 6 (2021) 723–732, https://doi.org/10.1038/s41560-021-00852-3.

[44] Y. Yamada, Y. Iriyama, T. Abe, Z. Ogumi, Kinetics of Lithium-ion transfer at the interface between graphite and liquid electrolytes: effects of solvent and surface film, Langmuir. 25 (2009) 12766–12770, https://doi.org/10.1021/la901829v.

[45] I.-J. Park, T.-H. Nam, J.-G. Kim, Diphenyloctyl phosphate as a solid electrolyte interphase forming additive for Li-ion batteries, J. Power Sources 244 (2013) 122–128, https://doi.org/10.1016/j.jpowsour.2013.03.031.

[46] H.S. Françon, Y.C. Gorur, C. Montanari, P.A. Larsson, L. Wågberg, Toward Li-ion graphite anodes with enhanced mechanical and electrochemical properties using binders from chemically modified cellulose fibers, ACS Appl. Energy Mater. 5 (2022) 9333–9342, https://doi.org/10.1021/acsaem.2c00525.

[47] J. Kim, S.M. Nithya Jeghan, G. Lee, Superior fast-charging capability of graphite anode via facile surface treatment for lithium-ion batteries, Microporous Mesoporous Mater. 305 (2020), 110325, https://doi.org/10.1016/j.micromeso.2020.110325.

[48] G. Ning, B. Haran, B.N. Popov, Capacity fade study of lithium-ion batteries cycled at high discharge rates, J. Power Sources 117 (2003) 160–169, https://doi.org/10.1016/S0378-7753(03)00029-6.

[49] S.H. Beheshti, M. Javanbakht, H. Omidvar, M.S. Hosen, A. Hubin, J. Van Mierlo, M. Berecibar, Development, retainment, and assessment of the graphite-electrolyte interphase in Li-ion batteries regarding the functionality of SEI-forming additives, IScience. 25 (2022), 103862, https://doi.org/10.1016/j.isci.2022.103862.

[50] W. Mei, L. Jiang, C. Liang, J. Sun, Q. Wang, Understanding of Li-plating on graphite electrode: detection, quantification and mechanism revelation, Energy Storage Mater. 41 (2021) 209–221, https://doi.org/10.1016/j.ensm.2021.06.013.

[51] A. Ransil, A.M. Belcher, Structural ceramic batteries using an earth-abundant inorganic waterglass binder, Nat. Commun. 12 (2021) 6494, https://doi.org/10.1038/s41467-021-26801-y.

[52] J.-B. Wu, M.-L. Lin, X. Cong, H.-N. Liu, P.-H. Tan, Raman spectroscopy of graphene-based materials and its applications in related devices, Chem. Soc. Rev. 47 (2018) 1822–1873, https://doi.org/10.1039/C6CS00915H.

[53] I.M. Alibe, K.A. Matori, H.A.A. Sidek, Y. Yaakob, U. Rashid, A.M. Alibe, M.H. M. Zaid, S. Nasir, M.M. Nasir, Effects of polyvinylpyrrolidone on structural and optical properties of willemite semiconductor nanoparticles by polymer thermal treatment method, J. Therm. Anal. Calorim. 136 (2019) 2249–2268, https://doi.org/10.1007/s10973-018-7874-7.

[54] Yuri Borodko, Susan E. Habas, Matthias Koebel, Peidong Yang, Heinz Frei, Gabor A. Somorjai, Probing the interaction of poly(vinylpyrrolidone) with platinum nanocrystals by UV-Raman and FTIR, J. Phys. Chem. B 110 (2006) 23052–23059.

[55] D.W. Matson, S.K. Sharma, J.A. Philpotts, The structure of high-silica alkali-silicate glasses. A Raman spectroscopic investigation, J. Non Cryst. Solids 58 (1983) 323–352, https://doi.org/10.1016/0022-3093(83)90032-7.

[56] C. le Losq, B.O. Mysen, G.D. Cody, Water and magmas: insights about the water solution mechanisms in alkali silicate melts from infrared, Raman, and 29Si solid-state NMR spectroscopies, Prog Earth Planet Sci 2 (2015) 22, https://doi.org/10.1186/s40645-015-0052-7.

[57] T. Furukawa, K.E. Fox, W.B. White, Raman spectroscopic investigation of the structure of silicate glasses. III. Raman intensities and structural units in sodium silicate glasses, J. Chem. Phys. 75 (1981) 3226–3237, https://doi.org/10.1063/1.442472.

[58] L. Giacomazzi, P. Umari, A. Pasquarello, Medium-range structure of vitreous SiO_2 obtained through first-principles investigation of vibrational spectra, Phys. Rev. B 79 (2009), 064202, https://doi.org/10.1103/PhysRevB.79.064202.

[59] K. Awazu, H. Kawazoe, Strained Si–O–Si bonds in amorphous SiO2 materials: a family member of active centers in radio, photo, and chemical responses, J. Appl. Phys. 94 (2003) 6243–6262, https://doi.org/10.1063/1.1618351.

[60] B.T. Young, C.C. Nguyen, A. Lobach, D.R. Heskett, J.C. Woicik, B.L. Lucht, Role of binders in solid electrolyte interphase formation in lithium-ion batteries studied with hard X-ray photoelectron spectroscopy, J. Mater. Res. 34 (2019) 97–106, https://doi.org/10.1557/jmr.2018.363.